Beam impedance minimization for accelerator beamline insertion devices

I. V. Konoplev, D. W. Posthuma De Boer, C. Warsop, and M. John

Published version information

Citation: IV Konoplev et al. "Beam impedance minimization for accelerator beamline insertion devices." Rev Sci Instrum 91, no. 7 (2020): 074711.

DOI: 10.1063/5.0007449

Review of Scientific Instruments

Beam impedance minimization for accelerator beamline insertion devices

Cite as: Rev. Sci. Instrum. **91**, 074711 (2020); https://doi.org/10.1063/5.0007449
Submitted: 12 March 2020 . Accepted: 23 June 2020 . Published Online: 21 July 2020

I. V. Konoplev, D. W. Posthuma De Boer, C. Warsop, and M. John

Review of Scientific Instruments ARTICLE scitation.org/journal/rsi

Beam impedance minimization for accelerator beamline insertion devices

Cite as: Rev. Sci. Instrum. 91, 074711 (2020); doi: 10.1063/5.0007449
Submitted: 12 March 2020 • Accepted: 23 June 2020 •
Published Online: 21 July 2020

I. V. Konoplev,[1,a)] D. W. Posthuma De Boer,[1,2] C. Warsop,[2] and M. John[1]

AFFILIATIONS

[1] Department of Physics, University of Oxford, Keble Road, Oxford OX1 3RH, United Kingdom
[2] ISIS, STFC RAL, Didcot OX11 0QX, United Kingdom

[a)] **Author to whom correspondence should be addressed:** ivan.konoplev@physics.ox.ac.uk

ABSTRACT

Use of complex state-of-the art detectors and monitors is essential to carry out high-energy and nuclear physics experiments at accelerator/collider facilities. The detectors are used to monitor charged particle beam parameters at large accelerator facilities such as coherent light sources and to develop new state-of-the art accelerators. Improvements in beam quality and lifetime necessitate the advancement of the instrumentation for successful operation of the accelerator facilities. Minimization of the beam-line-inserted devices' influence on the beam is therefore one of the essential considerations during the design of such facilities and the preparation of experiments. In this paper, we suggest and discuss a roadmap to minimize this influence. It is developed using fundamental concepts and numerical modeling, and we show that this is a multi-stage and multi-parametric problem that needs careful consideration. To illustrate the roadmap, the vacuum vessel for the vertex locator detector (CERN) is used. The results are discussed and, using them, the steps and stages of the design optimization are suggested. The suggested procedure can be applied to optimize the design of any beamline insertion device and will contribute to the development of next generation particle/accelerator detectors and monitors.

I. INTRODUCTION

State-of-the art beam detectors and monitors are indispensable for high energy and nuclear physics research, development of the new accelerators, monitoring charged beam parameters at light sources, and industrial and healthcare applications.[1–10] The number of the detectors used is growing, and they are becoming more sophisticated and complex. Recent and future facilities will have even more stringent requirements on beam stability, bunch lengths, transverse dimensions, and beam powers, meaning that more accurate and less invasive detectors will be required. The detectors are usually placed along the charged particle beamline, interrupting the continuity of the vacuum transport line while allowing the monitoring of the beams and products of the experiments, for example, from beam-target collisions.

The insertions of the devices lead to the excitation of wake electro-magnetic (EM) fields, which negatively impact the beam stability and its lifetime.[11] Evaluation of the excitation of these EM fields and their impact on the beam stability and the detector outputs are an important consideration during the design stage of the monitors. These studies are particularly important at storage ring facilities such as the Large Hadron Collider (LHC, CERN), which often require beams to circulate for many hours, traversing the monitors many times. The interaction of the charged particle beam with its surroundings is quantified by the beam coupling impedance. If this parameter is not minimized, it may lead to either distortion of the beam or even beam loss. To prevent beam instabilities,[11] EM wakefields are often suppressed or, equivalently, beam coupling impedances are reduced.[12] Modern accelerator facilities have impedance "budgets," which place strict limits on the beam impedance where each piece of experimental equipment can contribute.[2–5] The unwanted impedances can sometimes be mitigated during the design phase by relatively minor changes. Nevertheless, the impedance minimization is a challenge as it is a multi-parametric problem, which often requires significant computational resources.[12] Most of the detectors are hosted inside vacuum vessels, which are usually barrel shaped (large metal cylinders) with technical ports (Fig. 1). The geometry of the vessel impacts the beam

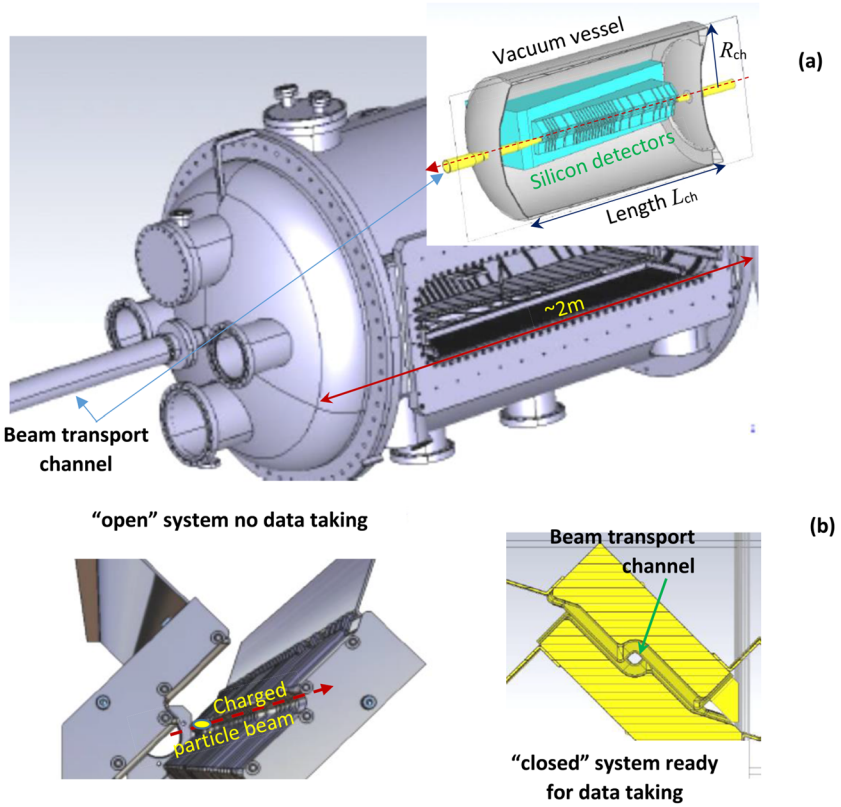

FIG. 1. (a) Technical drawing of the vacuum vessel for the VELO detector.[2,4] The inset shows the cross section of the simplified model of the vacuum vessel for the VELO detector.[2,4] The block inside the vessel illustrates the schematic of the silicon detectors housing and the beam transport channel. (b) The beam channel forms a "closed" pipe (right) during data taking, and it is "open" (left) as data taking is stopped.

coupling impedance,[2–5,12] and it is one of the primary sources of the impedance. A careful design of the vessel can reduce the overall impedance of the detector, increasing the life-time and the quality of the beam.

In this paper, a roadmap to design a low impedance vacuum vessel will be discussed. To start, as an example, we look at the current design of the Vertex Locator (VELO) vacuum vessel, which hosts the detector [silicon detectors developed for LHC (CERN)].[2,4] In Figs. 1(a) and 1(b), the parts of the design of the vacuum chamber and VELO detector are shown. The vessel houses detectors to study products of the beam–beam collisions. Its simplified numerical model (a cylindrical barrel with the beam pipe passing through its center with no technical ports or specific details), generated using CST MW Studio, is shown in the inset of Fig. 1(a).[2,4,13] The silicon detectors are hosted inside two aluminum containers, which are held on opposite sides of the beam; one of these containers is indicated by the "green block" in Fig. 1(a). The sides of the containers that face the beam and form the beam channel are indicated as a "gold pipe." The aluminum containers provide the RF shielding necessary to protect the silicon detectors. The beam channel formed during data taking [Fig. 1(b), right] operates as the EM shield. When the monitor is not taking data, the detectors are retracted breaking up the transport channel and EM shielding [Fig. 1(b), left] and forming two-conductor open lines with the charged particle beam propagating in the middle. Such a complex configuration of the monitor requires the EM optimization of the vacuum vessel to reduce the beam impedances.

We note that in the absence of the beam shielding, the vacuum vessel acts as a RF cavity, and while any vacuum vessel used to host a detector has specific features such as the technical ports, their absence in the model will not affect the discussions and the roadmap's basic principles. Here, we will study and discuss the EM properties of the vessel, i.e., the eigenmodes' field structures and their impedances and procedures to tune the vessel impedances, minimizing their impact and making the detector suitable for installation and use.

II. MODEL AND BEAM IMPEDANCE MINIMIZATION

The beam propagating through an RF cavity excites its eigenmodes, and to understand the properties of the eigenmodes that define the beam impedance, a simplified model of the vessel can be used (Fig. 1, inset). The length of the vessel (an RF cavity) L_{ch} affects the eigenmode density, and to simplify the analysis further making the discussions clear while maintaining the results' generality, a short cavity model (see insets of Fig. 2) will be used (radius R_{ch} = 200 mm, length L_{ch} = 80 mm, and beam pipe diameter D_p = 60 mm). The EM fields excited by the charged particle beam inside the cavity can be presented as a sum of the cavity eigenmodes as[14,15]

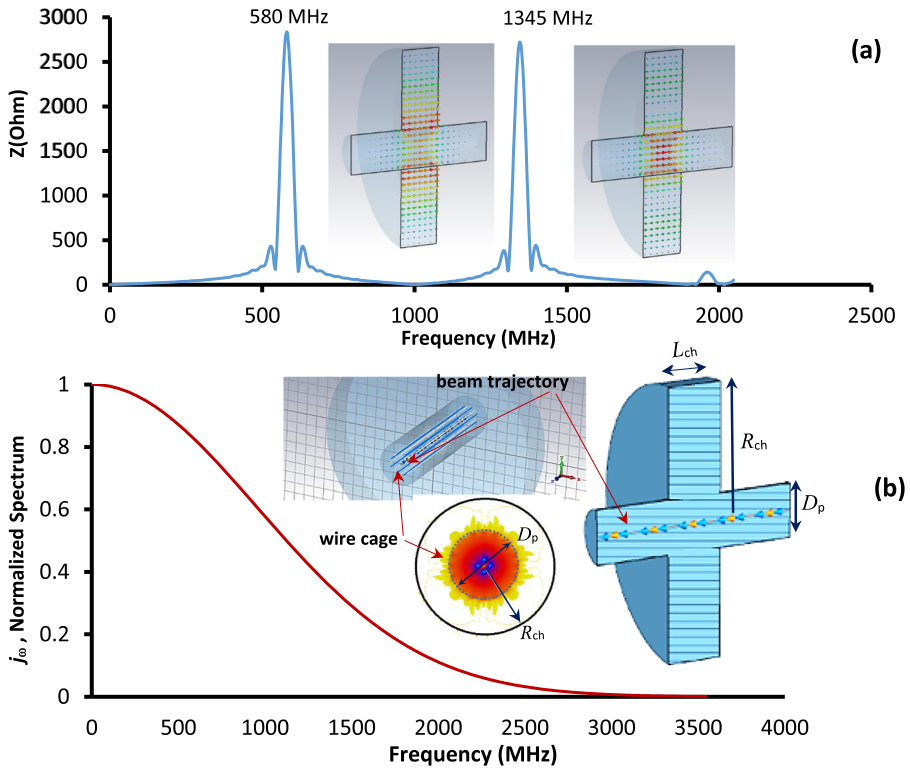

FIG. 2. (a) The magnitudes of the total impedances of the cavity in the frequency range from 0.01 MHz to 2000 MHz excited by the ideal beam propagating along the center of the cavity. The insets show the 3D contour plots of the modes' electric fields' at 580 MHz and 1345 MHz. (b) The electron bunch normalized spectrum/form factor assuming the Gaussian distribution of the particles. The insets show the drawing of the conventional cylindrical cavity (the cavity radius R_{ch} = 200 mm and length L_{ch} = 80 mm) with the beam pipe (diameter D_p = 60 mm) and the beam trajectory indicated. The schematic of the beam shielding with the set of thin wires running parallel to the beam is shown, and the contour plots illustrate the rapid decay of the electric field after the wire cage.

$$\boldsymbol{E} = \sum_s C_s \boldsymbol{E}_s, \quad \boldsymbol{H} = \sum_s B_s \boldsymbol{H}_s, \tag{1}$$

where $\boldsymbol{E}_s$ and $\boldsymbol{H}_s$ are the vectors of the electric and magnetic fields of the cavity eigenmodes (the bold letters show three-vectors), respectively, and C_s and B_s are constants that are generally not equal to each other if $\omega \neq \omega_s$ and $B_s \approx C_s$ if $\omega \approx \omega_s$. Here, ω is the variable, angular frequency of the EM radiation, and ω_s is the cavity eigenfrequency. Here, we will consider the latter case since the large beam coupling impedances occur at cavity resonances, as shown in Fig. 2(a), where the peaks of the impedances are coincident with the positions of the vessel's eigenmodes. The absolute values of the constants C_s in the expression (1) are defined in terms of the beam current and eigenmode structure as[14,15]

$$|C_s| = \left| \frac{\omega}{(\omega_s^2 - \omega^2)N_s} \int \boldsymbol{j} \cdot \boldsymbol{E}_s d^3x \right| \cong \left| \frac{1}{2\Delta\omega N_s} \int \boldsymbol{j} \cdot \boldsymbol{E}_s d^3x \right|, \tag{2}$$

where $N_s = -\frac{1}{4\pi} \int H_s^2 dV$ is the norm of the eigenmode. We assumed that $\varepsilon = \mu = 1$, $\boldsymbol{j} \cdot \boldsymbol{E}_s$ is the vector dot product of the beam current density and the eigenmode's electric field, and $\Delta\omega = (\omega - \omega_s)$ is the frequency detuning. The total impedance, which is a voltage to current ratio ($Z = U/I$), for the eigenmode with index s is given as

$$|Z_s(\omega)| = \left| \frac{U_s}{I} \right| = \left| \frac{\int_{-\infty}^{\infty} C_s \boldsymbol{E}_s \boldsymbol{dr}}{I} \right|. \tag{3a}$$

Taking into account that $\boldsymbol{dr} = \boldsymbol{dz} + \boldsymbol{dr}_\perp$, one can find the longitudinal and transverse impedances[15,16]

$$|Z_{s||}(\omega)| = \left| \frac{U_{s,z}}{I_z} \right| = \left| \frac{\int_{-\infty}^{\infty} C_s \boldsymbol{E}_s \boldsymbol{dz}}{I_z} \right|,$$
$$|Z_{s\perp}(\omega)| = \left| \frac{U_{s,\perp}}{I_\perp} \right| = \left| \frac{\int_{-\infty}^{\infty} C_s \boldsymbol{E}_s \boldsymbol{dr}_\perp}{I_\perp} \right|, \tag{3b}$$

where the integral is taken along the path of the beam and $I_{z,\perp} = \int \boldsymbol{j} \cdot d^2\boldsymbol{\sigma}$ (integral over the cross section $\boldsymbol{\sigma}$ with its normal vector parallel to $\boldsymbol{j}$) are the longitudinal and transverse currents. The total impedance (the sum of transverse and longitudinal impedances) is an indication of the total strength of the beam and cavity eigenmode coupling. This allows us to compare couplings on- and off-axis of the system without losing any generality, while for each specific design, the impedances (longitudinal and transverse) may have to be considered separately depending on the impedance budget allowances and other design conditions. Figure 2(a) shows the total effective impedances (CST MW Studio[13] is used to study the models) of the two fundamental modes excited by the beam propagating through the center of the cavity. The insets of Fig. 2(a) show the transverse field structures of the modes located at 580 MHz and 1345 MHz. Taking into account (2) and (3), we note that if $\boldsymbol{E}_s \to 0$, $\boldsymbol{j} \to 0$ or $\boldsymbol{j} \cdot \boldsymbol{E}_s \to 0$, the impedances will also tend to zero. A single bunch form factor is $\boldsymbol{j}_\omega(\omega) = \frac{1}{2\pi} \int_{-\infty}^{\infty} \boldsymbol{j}(t) e^{-i\omega t} dt$ [Fig. 2(b)], and we note that all the impedances shown in this work are calculated assuming a constant beam spectrum $\boldsymbol{j}_\omega(\omega) = 1$, i.e., one needs to multiply the spectrum

of the impedances by the bunch form factor to get the values of the effective impedance relevant to a specific beam current.

Let us consider practical steps to minimize the impedance. The direct shielding of the beam from the cavity synonymous with $\boldsymbol{j} \to 0$ results in the effective impedance minimization, and such a shielding can be achieved by a set of wires. Shielding by a wire cage is illustrated in the inset of Fig. 2(b) where the blue lines indicate a series of wires running parallel to the propagation axis of the beam. The contour plots below the schematic diagram show that the wire shielding nearly zeros the electric field outside the region enclosed by the wires (dotted line), and as a result, the impedances have been significantly reduced. However, in most cases, such shielding cannot be applied for a number of reasons, including beam interaction with the wires and secondary electron emission from the wires. Assuming that direct beam shielding cannot be applied, mismatching of the beam and vessel eigenspectra will also reduce the effective impedance. In Fig. 2(b), an example of the normalized spectrum of a single bunch that has a Gaussian charge distribution is shown. If the beam current is a periodic function, i.e., a set of the bunches, the current density can be presented as

$$\boldsymbol{j} = \sum_{s'} D_{s'} \boldsymbol{j}_{s'}, \tag{4}$$

where $D_{s'} = \frac{1}{2\pi} \int_{-\infty}^{\infty} \boldsymbol{j}(t) e^{-i\omega_{s'} t} dt$, and in the case of a train of Gaussian bunches, the spectrum will have a set of peaks,[17] which will appear at $\omega_{s'}$, i.e., a quasi-discrete spectrum. The peaks will have the amplitudes defined by the envelope shown [Fig. 2(b)], and the width of the peaks will be inversely proportional to the number of bunches, i.e., if the number is large (e.g., several thousands), the peak will be very narrow.

Looking at (1) and (4), we note that, in general, $s' \neq s$ and $\omega_{s'} \neq \omega_s$, while (2) and (3) are not zero only if $\omega_{s'} = \omega_s$. As a result, to minimize the effective impedance, the detuning of the beam spectrum maxima from the maxima of the cavity eigenmodes is desirable. In addition, the typical spectrum envelope decays from low to high frequencies [Fig. 2(b)], and shifting the cavity's eigenmodes to higher frequencies will help to minimize the effective beam impedances. One can note that the spectrum density of the real vessel is very high due to its large dimensions, i.e., there are always the cases $\omega_{s'} \cong \omega_s$. As such, the overlap of the vessel's eigenmode spectrum $f_\omega(\omega)$ with the spectrum of the beam $j_\omega(\omega)$ is difficult to avoid. Optimizing the vessel geometry in such a way to observe a minimum value of the two spectra convolution, $\partial_\omega(j_\omega(\omega) * f_\omega(\omega)) = 0$, will help to minimize the effective impedance. In a perfectly conducting vessel, a relatively small deviation from the original shape will result in the frequency shift,[15]

$$\frac{\omega^2 - \omega_s^2}{\omega_s^2} = \frac{\int_{\Delta V} (|H_s|^2 - |E_s|^2) d^3x}{\int_V (|H_s|^2) d^3x} \cong \frac{2\Delta\omega}{\omega_s}, \tag{5}$$

where ΔV and V are the deviation from the original volume and the original volume of the cavity, respectively, while the integrations are taken over the total volume and $\Delta\omega = \omega - \omega_s$. Equation (5) indicates that changing the cavity geometry leads to either positive or negative shifts of the eigenfrequencies, allowing the vessel spectrum to be tuned in a controllable and precise manner. In Fig. 3(a), the drawings of the modified cylindrical vessels M1 and M2 are shown.

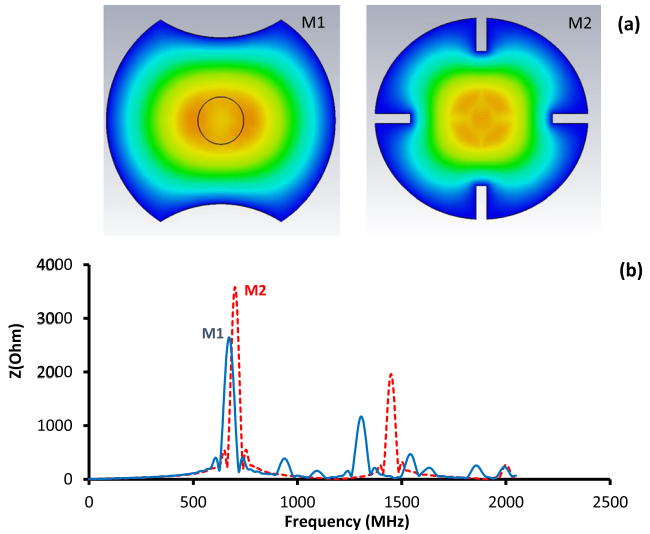

FIG. 3. (a) The contour plots of the first eigenmode structures in the modified cavities. Orange indicates the highest intensity field, and yellow, green, cyan, and dark blue show the gradual decay of the field intensities from high (yellow) to low (dark blue), respectively; (b) the magnitudes of the total impedances of the cavity in the frequency range from 0.01 MHz to 2000 MHz observed for the cavities M1 (solid line) and M2 (dashed line) with the beam propagating along the cavity center.

The mechanical deformations are as follows: smooth "cylinder-like" (M1) and "fin-like" (M2) recesses have been made to illustrate the possibility to perform the positive and negative shifts of the eigenmodes predicted by Eq. (5). If the changes are made on the cavity surface [as shown in Fig. 3(a)], the fundamental mode will always experience a shift to higher frequencies as the electric field's $|E_s|$ highest intensity is in the center of the cavity. As a result, the fundamental modes for the M1 and M2 cavities are shifted from 580 MHz to 675 MHz and to 702 MHz, respectively. The shifts of the second eigenmodes depend on the shapes and positions of the indentations. In the case of a smooth and relatively shallow recess (cylinder shaped deformation of radius 200 mm for M1), the eigenmode experiences a shift to lower frequency from 1345 MHz to 1310 MHz, while the "fin-like" recess (M2) results in the shift of the eigenmode to a higher frequency of 1448 MHz. We note that the "exaggerated" modifications shown in Fig. 3(a) for M1 and M2 cavities are for illustration purpose only to demonstrate "visible" shifts and application of the expression (5). More realistic cavities can be manufactured by making small recesses affecting accurately the positions of the eigenmodes as desired taking into account good understanding of the charge particle beam properties.

III. NEW METHODOLOGY FOR THE BEAM IMPEDANCE MINIMIZATION

We suggest using other opportunities to minimize expression (3) for a given beam (4) and variable parameters of the vessel defining the fields (1, 2) and develop an iterative methodology for the beam impedance minimization. Such a methodology will be

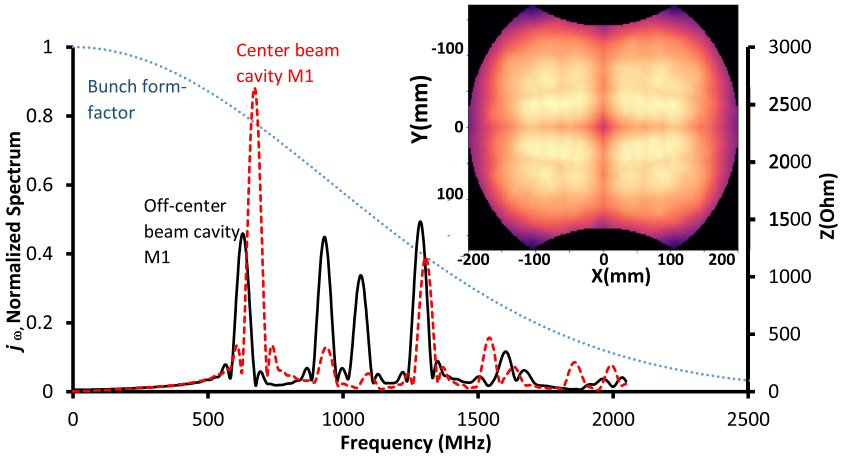

FIG. 4. The comparison of the magnitudes of the M1 cavity's total impedances is observed if the beam propagates through the center of the cavity (dashed line) and off-center of the cavity. The dotted line indicates the charged particles' bunch normalized spectrum. The inset shows the contour plot of the superposition of the eigenmodes fields (0.01 MHz–2000 MHz), i.e., $\sum_s \left\{\sqrt{E_{sz}^2} + \mu c\sqrt{H_{sx}^2 + H_{sy}^2}\right\}$ of the cavity M1, and the bright light colors indicate high amplitudes, and the dark colors show low amplitudes.

required to move from an idealized model discussed above to the technical design, as shown in Fig. 1.

Figure 3 shows that variations of the cavity geometry lead to the changes of the modes' transverse profiles. Using this property, the impedances can be decreased by minimizing $\boldsymbol{E}_s$ [see expression (3)] along the beam trajectory. The contour plots [Fig. 3(a)] illustrate the transverse structures of the fundamental modes. The electric field of the M1 cavity's eigenmode has a local minimum in

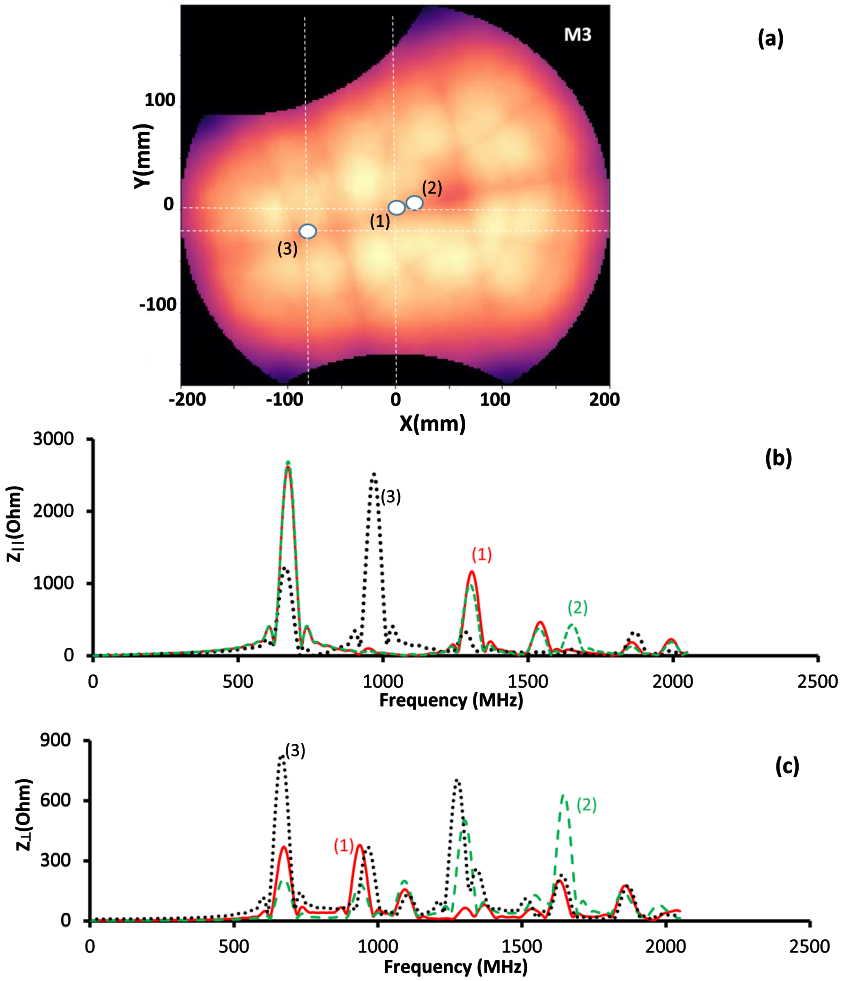

FIG. 5. (a) The contour plot of the superposition of the eigenmodes' fields (0.01 MHz–2000 MHz), i.e., $\sum_s \left\{\sqrt{E_{sz}^2} + \mu c\sqrt{H_{sx}^2 + H_{sy}^2}\right\}$ of the asymmetric cavity (M3). The bright light colors indicate high amplitudes, and the dark colors show low amplitudes. The dots indicate the (X, Y) positions of the beamline in the cavity: (1) X = 0 mm, Y = 0 mm; (2) X = 16 mm, Y = 5 mm; and (3) X = −80 mm, Y = −20 mm. The comparison of the longitudinal (b) and transverse (c) impedances observed for three beamline locations.

the center, leading [as expected from (3)] to a smaller amplitude of the coupling impedance for this mode of 2500 Ω as compared to 3500 Ω obtained for the M2 cavity. To further minimize $\boldsymbol{E}_s$, the beam path from the cavity center can be shifted to where the field strength is smaller. In Fig. 4, the mode impedances of the beam propagating through the center (dashed line) and off-center (solid line) of the cavity M1 are presented together with the bunch normalized form factor. The impedance of the fundamental mode has been reduced by a factor of 2.5; however, high order modes (HOMs) appear. The inset of Fig. 4 shows that the sum of the electric and magnetic fields $F = \sum_s \left\{\sqrt{E_{sz}^2} + \mu c\sqrt{H_{sx}^2 + H_{sy}^2}\right\}$ of the eigenmodes of interest in the frequency range from 0.01 MHz to 2 GHz acting on the charged particles in cavity M1 is shown. In this figure, the fundamental mode is overshadowed by the sum of the fields of the HOMs. Figure 4 and inset clearly show that positioning the beam off-center in the symmetrical vessel will result in the excitation of the upshifted HOMs, while putting the beamline in the middle is an optimal solution to avoid the excitation of these HOMs. The upshifted HOMs have lower impedances than the fundamental mode, meaning that their impact on the beam properties will be reduced. To further minimize the HOMs' impact an asymmetric vessel [an example is shown in Fig. 5(a)] can be used. In this case, the beam position can be further optimized to reduce the amplitudes of the impedances. We note that the deformation of the cylindrical vessel shape shown in Fig. 5(a) has been exaggerated for illustration purposes, and it is not a final or optimized shape of the vacuum vessel. In Figs. 5(b) and 5(c), the dependencies of the longitudinal (along the z coordinate) and transverse (along X and Y coordinates) impedances are shown for different beamline positions in the (X, Y) plane, as indicated in Fig. 5(a) by the white dots. Moving the beam from the center to point 3 (X = −80 mm, Y = −20 mm) has improved the longitudinal impedance most significantly especially for the first mode (from 2700 Ω to around 1000); however, the transverse impedance was increased. The small shift from center point 1 (X = 0 mm; Y = 0 mm) to point 2 (X = 16 mm, Y = 5 mm) also led to an impedance variation but not as significant. To sum up, Fig. 6(a) shows the total impedances for the asymmetric cavity if the beam passes through the points (1) solid line, (2) dashed line, and (3) dotted line. It is clear that the impact of the vessel on the beam property can be reduced by optimizing the beam position. In Fig. 6(b), the impedances for symmetric cavities (M1: dotted line, M2: dashed line) with the beam propagating through their centers and for the asymmetric vessel (M3: dotted line) with the beam propagating through point 3 are shown. As a result, by changing the configuration of the vessel and the beam's position inside the vessel, the values of the impedances can also be controlled and optimized.

To summarize, the effect of the effective impedances on beam dynamics can be mitigated by (1) detuning the cavity and the beam such that $\omega_{s'} \neq \omega_s$ (a special design of the cavity geometry and mechanical tuning, and this can be considered as indirect beam shielding); (2) shifting the cavity eigenfrequency spectrum to the higher end of the beam spectrum [minimizing the dot product in Eq. (2) and thus C_s in expression (3)]; (3) direct shielding of the beam $\boldsymbol{j} \to 0$ [if possible as shown in Fig. 1 and the inset of Fig. 2(b)]; and (4) reducing $\boldsymbol{E}_s$ values along the beam trajectories [reducing both dot product in (2) and $\boldsymbol{E}_s$ in (3)]. To carry out the effective impedance optimization, the following iterative steps should be considered: design an RF vacuum chamber and position the beamline at the minimum of the fields, introduce ports and other features to the cavity and repeat the optimization, introduce the detector inside the vacuum chamber, and complete the design. The completion of these steps will allow the design and building of detectors

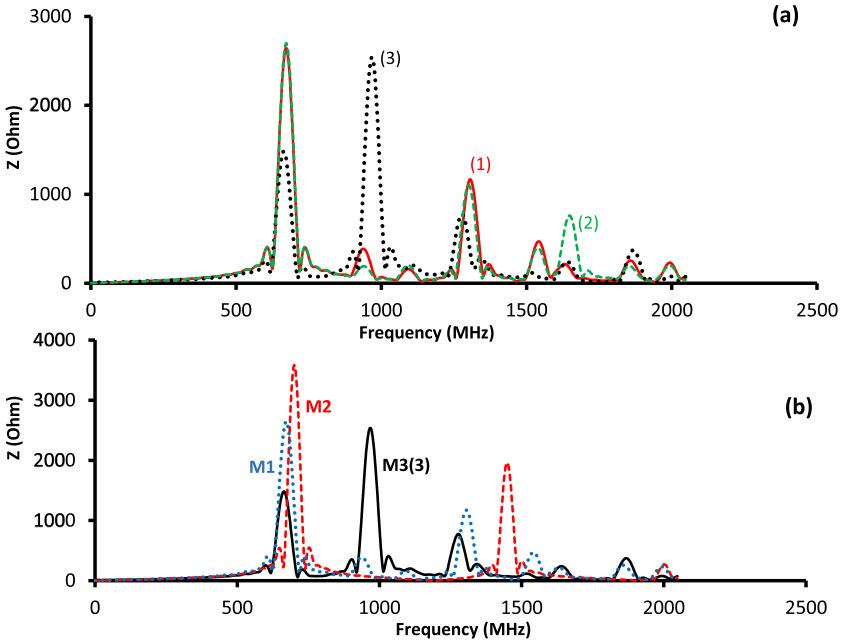

FIG. 6. (a) The comparison of the total impedances observed in the cavity M3 if the beamline center is located at point (1)—solid line, point (2)—dashed line, and point (3)—dotted line. (b) The comparison of the total impedances observed for symmetric cavities M1—dashed line, and M2— dotted line, if the beam propagates through the cavities' centers. The solid line shows the total impedance observed for the cavity M3 if the beam propagates off-center through point 3.

with the impedances below the values needed to maintain the beam quality and make the next generation of monitors "invisible" for the beams.

IV. CONCLUSION

The design of a detector with low effective impedance is a multistage problem in which the RF vacuum vessel design should be one of the first steps. Introduction of a dielectric inside the cavity will shift the modes and change their impedances. Considering the recent developments of the EM software[13] and numerical capabilities, tasks of a similar complexity, for example to optimize LHC collimators,[12] next generation antennas, surface-structured cavities, and superconducting RF cavities,[18–20] have already been carried out, illustrating that vessel optimization to reduce the detector's impedance is possible. The roadmap to carry out the effective impedance optimization and the steps and methodology have been suggested and discussed. The importance of the careful design of the RF vacuum chamber and position of the beamline at the minimum of the fields has been shown, and we suggest that the best way for impedance minimization is an iterative process from a simple model to the final technical design. The completion of the optimization process will allow the design and building of the detectors with the impedances below the values needed to maintain the beam quality required for the accelerator facilities. The methodology suggested will advance the development of the next generation of beam monitors and detectors by minimizing their impedances, which will improve beam quality and reduce energy consumption and run the costs of large facilities.

ACKNOWLEDGMENTS

The authors would like to thank colleagues from CERN for stimulating this work and STFC UK for the partial support of this work.

DATA AVAILABILITY

The data that support the findings of this study are available from the corresponding author upon reasonable request.

REFERENCES

[1]LHCb Collaboration *et al.*, LHCb reoptimized detector design and performance: Technical Design Report (CERN-LHCC-2003-030; LHCb-TDR-9) (2003), available at http://cds.cern.ch/record/630827.

[2]M. Williams, "Upgrade of the LHCb VELO detector," J. Instrum. **12**, C01020 (2017).

[3]M. Benedikt, M. Capeans Garrido, F. Cerutti *et al.*, Future Circular Collider–Vol. 3: The Hadron Collider (FCC-hh), Technical Report CERN-ACC-2018-0058, CERN, Geneva, December 2018, available at https://cds.cern.ch/record/2651300; R. Abela, K. Witte, A. Schwarz, H. Redlin, H.-J. Eckoldt, M. Hartrott, K. Floettmann, M. Fajardo, V. Katalev, T. Schilcher *et al.*, "XFEL: The European X-ray free-electron laser—Technical design report," Technical Report PHPPUBDB-14956, DESY, 2006; S. Peggs and European Spallation Source, ESS Conceptual Design Report, ESS, Lund, ESS-2012-001 (2012), available at https://europeanspallationsource.se/sites/default/files/downloads/2017/09/CDR_final_120206.pdf.

[4]LHCb Collaboration *et al.*, "The LHCb detector at the LHC," J. Instrum. **3**, S08005 (2008).

[5]J. L. Pellegrini, "A review of accelerator instrumentation," in Proceedings to 11th International Conference on High-Energy Accelerators, Geneva, Switzerland, July 7–11, 1980.

[6]K. P. Nesteruk, "Beam monitor detectors for medical applications," Rep. Pract. Oncol. Radiother. **19**, S32–S36 (2014).

[7]G. Andonian *et al.*, "Longitudinal profile diagnostic scheme with sub-femtosecond resolution for high-brightness electron beams," Phys. Rev. Spec. Top.–Accel. Beams **14**, 072802 (2011); H. L. Andrews *et al.*, *ibid.* **17**, 052802 (2014).

[8]N. Samadi, X. Shi, and D. Chapman, J. Synchrotron Radiat. **26**, 1863–1871 (2019); R. Voutta *et al.*, Phys. Rev. Accel. Beams **19**, 053201 (2016).

[9]K. Tiedtke *et al.*, "The SASE FEL at DESY: Photon beam diagnostics for the user facility," AIP Conf. Proc. **705**, 588 (2004).

[10]S. Z. Green *et al.*, "Beam diagnostic challenges for facet-II," IBIC2017, MO3AB3, Grand Rapids, MI, USA, 2017.

[11]B. Zotter and A. Kheifets, *Impedances and Wakes in High Energy Particle Accelerators* (World Scientific, Singapore, 1998); A. W. Chao, *Physics of Collective Beam Instabilities in High Energy Accelerators* (Wiley, New York, 1993); R. Williamson, B. Jones, and C. Warsop, in *Proceedings to 57th ICFA Advanced Beam Dynamics Workshop on High-Intensity and High-Brightness Hadron Beams (HB'16)*, Malmö, Sweden, July 3–8, 2016, http://www.jacow.org, pp. 155–159; M. M. Karliner, N. V. Mityanina, B. Z. Persov, and V. P. Yakovlev, Part. Accel. **50**, 153 (1995).

[12]A. Burov and V. Danilov, "Suppression of transverse bunch instabilities by asymmetries in the chamber geometry," Phys. Rev. Lett. **82**(11), 2286 (1999); N. Mounet, "Vlasov solvers and macroparticle simulations," Report CERN-2018-003-CP, CERN, Geneva, Switzerland, 2018; N. Biancacci, F. Caspers, J. Kuczerowski, E. Métral, N. Mounet, B. Salvant, A. Mostacci, O. Frasciello, and M. Zobov, Phys. Rev. Accel. Beams **20**, 011003 (2017); B. Salvant, D. Amorim, S. Antipov, S. Arsenyev *et al.*, "Building the impedance model of a real machine," in *10th International Particle Accelerator Conference, IPAC2019, WEYPLS1*, Melbourne, Australia, 2019, http://www.jacow.org, pp. 2249–2254.

[13]See https://www.cst.com for CST.

[14]J. D. Jackson, *Classical Electrodynamics* (John Wiley & Sons, Inc., 1962); R. E. Collin, *Foundations for Microwave Engineering* (IEEE Press, New York, 2001).

[15]L. D. Landau and E. M. Lifshitz, *Electrodynamics of Continuous Media* (Nauka, Moscow, 1992); D. M. Pozar, *Microwave Engineering* (John Wiley & Sons, Hoboken, NJ, 2011).

[16]H. Okamoto, S. Jiang, and R. L. Gluckstern, "Longitudinal and transverse impedance of an iris in a beam pipe," Phys. Rev. E **50**, 1501–1515 (1994).

[17]F. B. Taheri *et al.*, "Electron bunch profile reconstruction based on phase-constrained iterative algorithm," Phys. Rev. Accel. Beams **19**, 032801 (2016); H. Zhang *et al.*, "Non-destructive measurement and monitoring of separation of charged particle micro-bunches." Appl. Phys. Lett. **111**, 043505 (2017).

[18]Z. D. Zaharis *et al.*, "Design of a novel antenna array beamformer using neural networks trained by modified adaptive dispersion invasive weed optimization based data," IEEE Trans. Broadcast. **59**(3), 455–460 (2013); V. Grout *et al.*, "Software solutions for antenna design exploration," IEEE Antennas Propag. Mag. **61**(3), 48–59 (2019).

[19]A. J. MacLachlan *et al.*, "Resonant excitation of volume and surface fields on complex electrodynamic surfaces," Phys. Rev. Appl. **11**, 034034 (2019).

[20]R. Ainsworth *et al.*, "Asymmetric dual axis energy recovery linac for ultrahigh flux sources of coherent x-ray and THz radiation: Investigations towards its ultimate performance," Phys. Rev. Accel. Beams **19**, 083502 (2016).